PERGAMON

Micron 30 (1999) 267–276

micron

www.elsevier.com/locate/micron

TEM sample preparation by ion milling/amorphization

Á. Barna, B. Pécz*, M. Menyhard

Research Institute for Technical Physics and Materials Science, Hungarian Academy of Sciences, P.O. Box 49, H-1525 Budapest, Hungary

Received 27 October 1998; received in revised form 11 January 1999; accepted 18 January 1999

Abstract

Artefacts evolved during TEM sample preparation by ion milling are discussed. Possibilities are given to minimise the amorphization/damage of the ion milled samples. A new type of low energy ion gun is applied in the ion milling device; ion beam induced artefacts are minimised, as shown for samples of GaAs and Si.

Keywords: Ion milling; Electron microscopy; Damage; Amorphization; Ion gun

1. Introduction

TEM (Transmission Electron Microscopy) is a powerful technique for the investigation of a wide range of materials, effects of different treatments, solid state reactions, etc. The limiting factor in the exploration of the real structure of samples by this method is often sample preparation, instead of the resolution of the electron microscope (Kestel, 1995; Hytch and Chevalier, 1994).

TEM characterisation needs a thin section of the material that is transparent to the electron beam. Although adequate chemical etching procedures are available for some materials to prepare TEM samples, ion milling is used widely nowadays because more and more complex materials should be studied, for which uniform chemical etching conditions are not known, while ion milling can be applied to a wide range of different materials. Therefore, independently of the artefacts it produces, ion milling has become a general sample preparation method. Artefacts produced by the electron beam during observation also should be taken into account (Brown and Humphreys, 1998).

A number of studies in ion implantation/ion beam modification of materials point out that the structure of the sample (the subject of the study) might become modified by energetic ions, and artefacts can be formed in this way. Although the applied energy of ion milling is relatively low (3–10 keV), formation of damage and thus the modification of the original sample structure should be considered when layers of the material are removed. A review of the damage caused by ion milling was published by Barber (1993). The sputtering behaviour of compound semiconductors was treated in detail by Malherbe (1994a, b). To avoid the misinterpretation of TEM results one should consider that ion milling can cause the formation of artefacts. For example, in the article of Carter et al. (1986) SiC/Si structures have been investigated and a thin amorphous layer has been found at the interface. Checking the thicker parts of the samples they concluded that this is an artefact produced by ion milling during TEM sample preparation. In this case close investigation of the SiC/Si interface was not possible. In some other studies, formation of amorphized regions was experienced, which lead to the misinterpretation of the results (implying that epitaxial layers were formed with an amorphous layer between the substrate and the overgrown crystalline layer).

Cleaved specimens for TEM are considered damage-free ones, however an amorphous edge of the sample typically appears on the HREM images (Buffat et al., 1988; Benaissa et al., 1994). This can be contamination of the sample, which hinders the exploration of the original structure.

Ion milling technique and devices, based on experimental results, were further developed and modified during the last 10 years. Sample rotation during thinning was the first method that became generally applied to get a smoother surface after sputtering. Later rocking mode and sector speed thinning methods were developed to prepare uniformly thin slices of layered structures exhibiting quite different sputtering rate for Ar^+ ions (Barna, 1992). By now the aforementioned techniques are included in all of the ion milling devices on the market. Some of them can be used in retarded field mode (Barna et al., 1997) as well, but for this application guns producing mainly ions instead of neutral particles are needed. Today all of the ion milling devices

* Corresponding author. Tel.: +36-1-395-9240; fax: +36-1-395-9284.
E-mail address: pecz@mfa.kfki.hu (B. Pécz)

0968-4328/99/$ - see front matter
PII: S0968-4328(99)00011-6

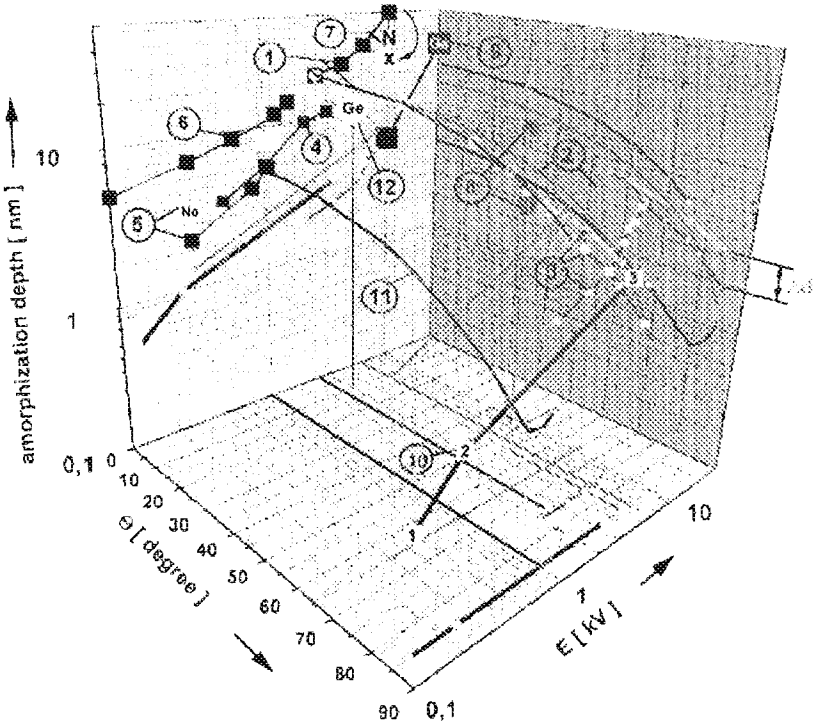

Fig. 1. Amorphization depth dependence on the beam incidence, Θ, and on the ion energy for Si single-crystal substrates bombarded by gas and metal ions (Ar if is not indicated). Curve No (12) relates to Ge. A detailed description of data are given in the text.

provide the possibility of low angle ion beam milling, which reduces the ion damage. In contrast, powerful ion guns are needed when low angle of incidence is applied. In commercially available devices the energy of the sputtering Ar^+ ions can be reduced down to 2 keV, but not further.

Although abundant literature was published on ion damage of different materials, most of them discuss the damage caused by ion implantation of high energy ions. Low energy studies (Hu et al., 1991; Kido and Nakano, 1990), however, deal with high angle beam incidence (close to the surface normal), therefore the above results can hardly be applied for the TEM sample preparation case, when low angle of incidence is applied.

The detailed analysis of the ion–solid interaction during bombardment is given by Menyhard in another paper of this volume. In this article we focus on the ion damage which is observed as an amorphous cover and edge on most TEM samples. We discuss the cases of silicon and GaAs. A survey of data found in the literature is given in the next part. Then we report on a new, low energy ion gun used for TEM sample preparation. Our results prove how the damaged layer thickness can be reduced by decreasing the ion energy.

2. Damage data in the literature on silicon and GaAs

In electron microscopy, ion damage appears in two main forms: first as changes in the surface topography, secondly as a damaged (typically amorphized) surface layer. Originally smooth surface topography can be preserved by sample rotation and by low angle of beam incidence (Barna et al., 1990). However, usually an amorphized surface layer is revealed by high resolution electron microscopy. The reduction or possibly the elimination of the surface damage is essential.

Indirect (RBS, ellipsometry, electrical measurements) and direct (HREM, STM, etc.) methods are available to investigate the ion damage bombarded samples. A summary of the literature on silicon and GaAs is given below.

2.1. Published data of damage on silicon

Fig. 1 shows the data we have found in the literature on the amorphous layer thickness produced by ions at different energies and angles of incidence (measured with respect to the sample surface normal). The astonishingly high scatter of the data is obvious. It is clear that few data on low energy and grazing angle of incidence have been published.

The data of the curves (numbered consequently in Fig. 1) are taken from the following articles:

1. Ishiguro et al., 1987. (Curve with experimental data is marked by black solid squares, the second one is marked by white spheres while the projection of the latter one is marked by small white circles.) Si (100) and (111) surfaces were bombarded by Ar ions in the above experiment and using a glow-discharge ion gun (in a JEOL/JIT-100 ion mill). Dependence of the

damage layer thickness on the orientation of the substrate was not observed. The damage layer thickness was measured by the ECP (electron channelling pattern) method (solid square). The result of the XTEM (cross-sectional TEM) measurement (marked by X in the square) does not show acceptable agreement with the data estimated by ECP. The reason for this may be the lattice distortion sensitivity of ECP or an artefact of the cross-sectional TEM sample preparation procedure (the amorphized Si surface might react with the glue material, for example).

2. Bulle-Lieuwma and Zalm, 1987. (Green curves.) The experiment was carried out in a Gatan/Dual Ion Mill Model 600 (glow discharge ion gun) on Si (100) and the damaged layer thicknesses were measured by TEM. In this curve the total damage layer thickness is given, e.g. the thickness of amorphous Si plus the thickness of the oxidised amorphous Si.
3. Schuhrke et al., 1992. (Wine-coloured curves show the experimental results, the white ones are calculated.) Gatan/Dual Ion Mill Model 600 was used for the experiment and data were measured by XTEM. Winterorn's tabulated data were used for calculation. A difference, Δd, between the experimental and calculated data should be note however the tendency in the measured and calculated data is the same.
4. Konomi et al., 1989. (Black squares mark the experimental data.) Damage layer thickness was measured on Si (100) by medium energy ion scattering (MEIS).
5. Buckner et al., 1988. (Data measured for Ar are marked by large, black, solid squares, while data for Ne is set in white.) The damage thickness in Si (100) created by Ne^+ and Ar^+ ions of a Kaufman-type ion source was measured by ellipsometry and Rutherford backscattering (RBS) methods.
6. Hu et al., 1991. (Large, black solid squares.) In situ ellipsometry was applied in this work to study the amorphization of single crystalline silicon by low energy Ar^+ ions (100–1500 eV). Here the total damage thickness is given by the amorphous region with voids plus amorphized silicon. Normal incidence of ions was applied. Although the above values are indirect data based on ellipsometric study, the formation of sample artefacts could be studied in this way.
7. Markwitz et al., 1996. (The measured single point is marked by a letter N in a solid square.) 10^{14} N ions/cm^2 were implanted into silicon and the damage depth was measured by XTEM.
8. Yokota et al., 1990. (Large, blue dots.) These measurements were carried out in a JEOL/JIT-100 ion mill and then by XTEM. Their results partially contradict the results of Ishiguro et al., 1987.
9. Walker and Broom, 1997. (Two purple solid squares.) Here the bombardment of Si was carried out by Ga ions (not by the generally used Ar ions) in a focused ion beam (FIB) device and the data shown were obtained by XTEM.
10. Barna et al., 1998. (Numbers in white solid squares, red curve.) High- and low-energy Teletwin ion guns were used. The bombarded samples were coated by a capping layer and the damage thickness was measured by XTEM.
11. Menyhard, 1999. (Continuous blue line.) Monte Carlo simulation (T-DYN code) of the damage depth.
12. Kido and Nakano, 1990. (Single, large dot marked by Ge.) This is the only experiment, shown here, which was carried out on Ge rather than Si. However, the above two elemental semiconductors show similar sputtering behaviour and this study should be mentioned. (A) Duoplasma ion source was applied. The extracted Ar^+ ion beam contains 8% of double ionised Ar^{++} ions. A 12–13 nm thick amorphous region was observed as a result of 3 keV Ar^+ ion irradiation. This was an ion implantation study carried out at a high angle of incidence. The damage depth was measured by MEIS.

The thickness of the amorphized region is proportional to $E \cos \Theta$, where E is the bombarding energy, Θ is the angle of beam incidence according to the results of Ishiguro et al. Other authors reported on square root energy dependence (Zalm and Vrizema, 1992; Bulle-Lieuwma and Zalm, 1987; Barna and Menyhard, 1994). Barna and Menyhard (1994) have found that only a weak, if any, dependence exists on the angle of the incidence, Θ, in the range of 80–89°.

Despite the confusing high scatter of the data in Fig. 1 and various possible dependencies one has to consider, some definite tendencies can be observed in the curves. The dependence of the amorphised depth on the angle of incidence (determined from measurements) can be described by cosine law if $\theta < 80°$. The ion energy dependence of amorphization for Si and noble gases follows a power law relationship between the linear and square-root dependence for the curves (1)–(6) and (10). Analysing the curve No. (9) (Walker and Broom, 1997) we can see that increasing the ion energy by a factor of three increased the damage depth by five times for silicon in the case of the Ga ion bombardement in a FIB unit. We should note, however, that the neutralisation probability depends on the type of ions. The noble gas ions neutralise upon readily entering the solid, while the metal atoms might keep their ionised condition much longer, resulting in a different range (Biersack, 1995).

Recently, ion milling devices for TEM sample preparation (Gatan, Technoorg-Linda etc.) or FIB units, applied for the same purpose, use a very low angle of beam incidence ($85° < \Theta > 90°$). However, we could not find experimental data in this angle-of-incidence range. The calculated data for increasing Θ (Schuhrke et al., curve No (3)) show increasing difference with respect to measured data (Δd, in Fig. 1). Also, the reality of the roll-off of the curves of the T-DYN Monte Carlo simulations (curve No (11) in Fig.

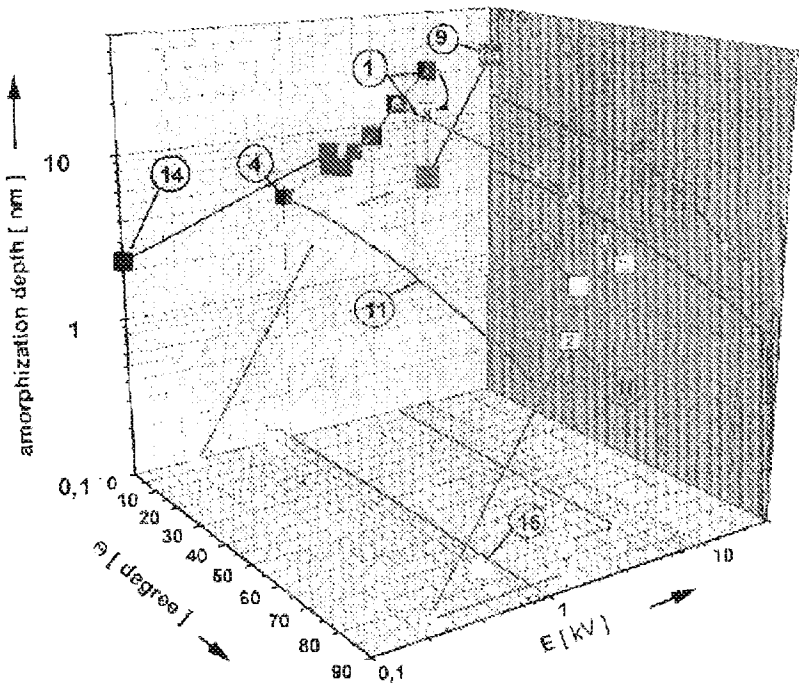

Fig. 2. Amorphization depth dependence (of GaAs single crystal substrates bombarded by Ar and metal ions) on the beam incidence, Θ, and on the ion energy. Detailed description is given in the text.

1) is questionable. This means that there are no experimental data for grazing angles of beam incidence and the calculated data are not reliable, despite this being the most important range of beam incidence needed to prepare good quality TEM samples.

2.2. Published data of damage on GaAs

The data found in the literature are summarised in Fig. 2. The data of curves No. (1), (4), (9), (10), (11) were published in the appropriate articles cited under the same number in the caption of Fig. 1. The experimental setup and the characterisation techniques were the same as for silicon. Data of the additional curves were taken from the following articles:

13. Ivey and Piercy, 1987. (White, solid squares, green line.) Gatan/Dual Ion Mill Model 600 and Ion Tech B304/404 Microlap ion mills (saddle-field ion gun) were used for the bombardment. The damage depth was measured by XTEM and calculated from Winterorn's tabulated data.
14. Kawabe et al., 1978. (Two large, black solid squares.) A Kaufman type gun served as a source of neutralised Ar beam. The damage layer depth was measured by RBS (2.3 nm at 0.1 keV and 7.2 nm at 2 keV).
15. Pearton et al., 1990. (Two large, white solid squares, orange line.) A Technics Micro Ion Mill, MIM (TLA 20) was used. The damage depth of GaAs bombarded by the neutralised Ar beam was calculated from I–V (current–voltage) characteristics and RBS.

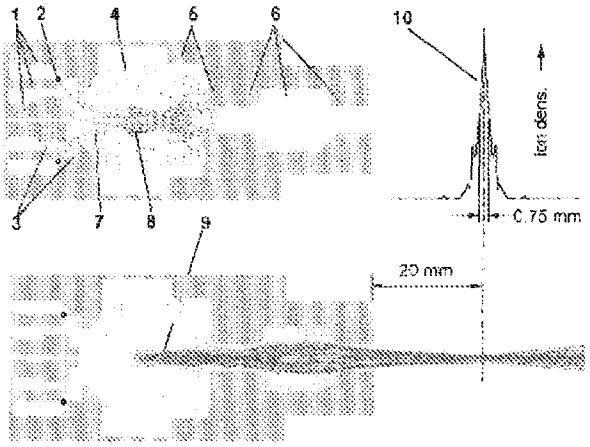

Fig. 3. Low-energy ion gun. 1: back side cold cathode system, 2: hot ring cathode, 3: adjusting electrode, 4: anode, 5: front side cold cathode system, 6: focusing lens system, 7: electron trajectory, 8: starting position of ions, 9: ion trajectory, 10: ion current density distribution at the sample position.

The difference found in the above data are too significant to observe any trend. The largest contradictory difference in Fig. 2 is between curves (14) (Kawabe et al.) and (15) (Pearton et al.) despite the fact that the samples were bombarded in both cases with neutralised Ar, and only the detection methods (RBS and I–V characteristic measurements and RBS) were partly different.

Both for elemental semiconductors and for GaAs, there is a high scatter in the published data. The main reason for this

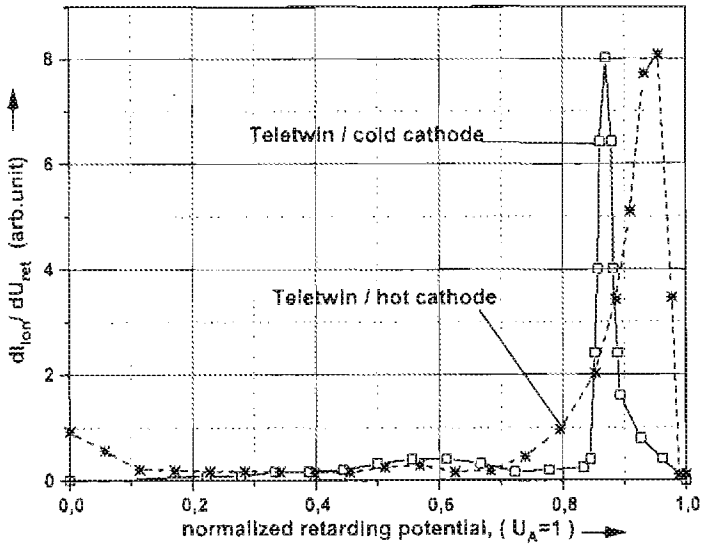

Fig. 4. Ion-energy distribution of the cold- and of the hot-cathode Teletwin guns.

may be the different ion sources used for the above experiments. In some of the ion sources, doubly ionised ions can be present and can create deeper damage. In some cases there is a large difference between the nominal voltage of the ion gun and the actual energy of the ions produced; thus caution is necessary for comparison of the data.

As mentioned, grazing-beam incidence is needed for polishing of the samples, but in that range no experimental results have been published in the literature. In contrast, the computer simulation gives unexpected results in this range (curve (11) in Fig. 1), which do not seem consistent with the next, higher angular range of beam incidence.

3. Low energy experiments

3.1. Construction of the low energy ion gun

A low energy (0.1–2 keV) ion gun (Fig. 3) has been developed, on the basis of the Teletwin ion gun (Barna et al., 1988) arrangement (working in the range of 2–10 keV), for TEM sample preparation and for sputtering in surface analytical equipment (AES, XPS etc.) (Barna and Szigethy, 1996).

Fig. 3 shows a sketch of the low-energy ion gun, including the electron and the ion trajectories according to a computer simulation. The electrons start from the hot ring cathode (2), and are focused into the axis of the anode (4). The electrons then turned back by an electrostatic mirror field (7), and a major part of them oscillate between the two cold cathodes (1,5). The process results in a high electron density around the axis of the anode. The electrons generate ions (8) accelerated into the cold cathode directions (only the trajectories of the ions leaving the gun to the front side direction are shown in Fig. 3). The focusing lens system (6) collects the ions onto the sample. The trajectories (9) and the ion current density distribution (10) were simulated at 300 V anode potential. The energy range of the ions is determined by the potentials of the anode and by the potentials of the retarding type focusing lens.

As mentioned already, one should determine the relationship between the nominal and actual energy of the ions produced by the ion gun (Crockett, 1972), otherwise comparison of the data might be confusing. Ion energy distribution was measured with a retarding energy analyser, for both the cold- and hot-cathode Teletwin guns (Fig. 4). (The cold cathode gun here means the high energy (2–10 keV) and hot cathode gun means the low energy (0.1–2 keV) ion guns.)

The main peak of ion-energy range appears for both guns over 85% of the nominal anode potential (U_A) value, being $0.87U_A$ and $0.96U_A$ for the cold- and for the hot-cathode guns, respectively. These data were measured at the nominal values of $U_A = 10$ kV for the cold-cathode and $U_A = 2$ kV for the hot-cathode gun. As the ion current of the hot cathode (low energy) gun is high, this gun can be used for thinning at low voltages within a reasonably short time. High ion current density is advantageous to avoid contamination (in a usual high vacuum system) as most of the ions impinging the sample surface will be the gas ions used for thinning (Carpenter et al., 1995).

3.2. Double ionisation

It is important to clarify whether double or multiple ionised particles are present or not in our ion beam, since the range might depend on the charge state due to the higher energy of the double ionised particle. However, Biersack (1993) studied, by means of TRIM simulations, the effect of electric charge on the stopping and range of ions of the

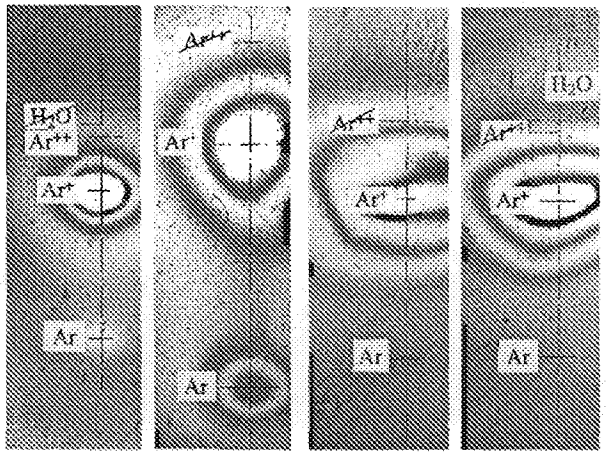

Fig. 5. Craters developed on the surface of oxidised silicon during bombardment by Teletwin ion guns. (a): cold cathode at 10 kV, (b): cold cathode at 3 kV, (c): hot cathode at 2 kV, (d): same as in (c), but without cooling trap. The position of the possible projectiles is indicated in the images; if one of them is not present, the appropriate label is set in strike-through letters.

same energy. He demonstrated that at high ion energies there is no dependence, but at low energies the range depends on the charge of the ion. Thus the actual ion charge must be carefully analysed. Sputtering experiments were carried out to determine the multiply ionised fraction of the ion beam, by bending the ion beams with small rare-earth magnets. Oxidised Si substrates were the targets in these experiments. In Fig. 5 the developed craters and the interference fringes due to the thickness changes in SiO_2 are shown.

Fig. 5(a) describes the behaviour of the cold-cathode gun. "Ion beam cathode" (90% of the beam is Ar^+ in this case) was used in the high energy Teletwin gun and a minimum Ar gas pressure was applied. The gun parameters were U_A = 10 kV, anode current I_A = 0.5 mA and ion current I_i = 30 μA. At these settings one can expect with the highest probability the generation of multiply charged ions. The main crater developed by Ar^+ ions and another crater produced by the neutralised Ar ions (fast Ar atoms, which makes about 10% of the beam) can be clearly seen in Fig. 5(a). There is a hardly-visible crater, indicated on the picture, developed at the position of double ionised Ar^{++}.

Fig. 5(b) refers also to the cold-cathode gun, with different sputtering parameters: U_A = 3 kV, anode current I_A = 2 mA and ion current I_i = 20 μA (usual settings for thinning). The craters created by Ar^+ ions and by neutralised Ar ions can also be seen clearly. However, the effect of Ar^{++} ions, in these conditions, was not detectable.

Fig. 5(c) describes the behaviour of the hot-cathode gun, (U_A = 2 kV, anode current I_A = 20 mA and ion current I_i = 30 μA, total residual pressure in the vacuum chamber 10^{-6} mbar). The crater developed by Ar^+ ions can be seen clearly, while a small crater developed by the neutralised Ar ions is also detected. Nothing is detected at the position of doubly ionised Ar ions. The expected positions of neutral and doubly ionised Ar are indicated in the picture as well.

Fig. 5(d) shows the crater created by the hot-cathode gun with the same setting as for Fig. 5(c), except for the value of the ambient pressure. In this experiment we did not use the liquid N_2 cooling trap, therefore a relatively high H_2O partial pressure appeared in the vacuum chamber ($p = 5 \times 10^{-6}$ mbar). Ion current in the range 1–2 μA was detected without Ar inlet into the ion gun. In Fig. 5(d) the sputtering contribution of H_2O is clearly detectable.

From the aforementioned experiments we could estimate that the doubly (or multiple) charged ion content of the ion beam of Teletwin ion guns is less than 1 -2% of the Ar^+ ions. The purity of the sputtering gas (contamination from chamber gas can appear inside the gun), is a strong requirement. According to our experience the sample surface can easily be oxidised during sputtering with a low energy gun, if air or H_2O penetrates into the gun.

3.3. Damages at low energy

The amorphised depth developed during the ion bombarding was determined by XTEM in our experiments. This is a direct method with the best resolution. However, there are several steps in the sample preparation process that might also introduce alteration of the surface and thus extreme care should be paid to the sample preparation. The very first step, removing the irradiated sample from the vacuum chamber to air, can already result in modification of the bombarded surface. Generally the damaged layer thickness is measured at the perforation edge of the sample.

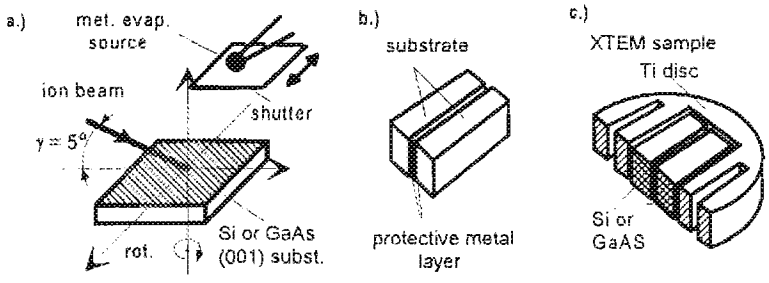

Fig. 6. Steps of TEM sample preparation. (a): Bombardment of the semiconductor surface and in situ deposition of a protective coating layer. (b): Small pieces are cut and positioned face to face. (c). The two small pieces are embedded into a Ti grid.

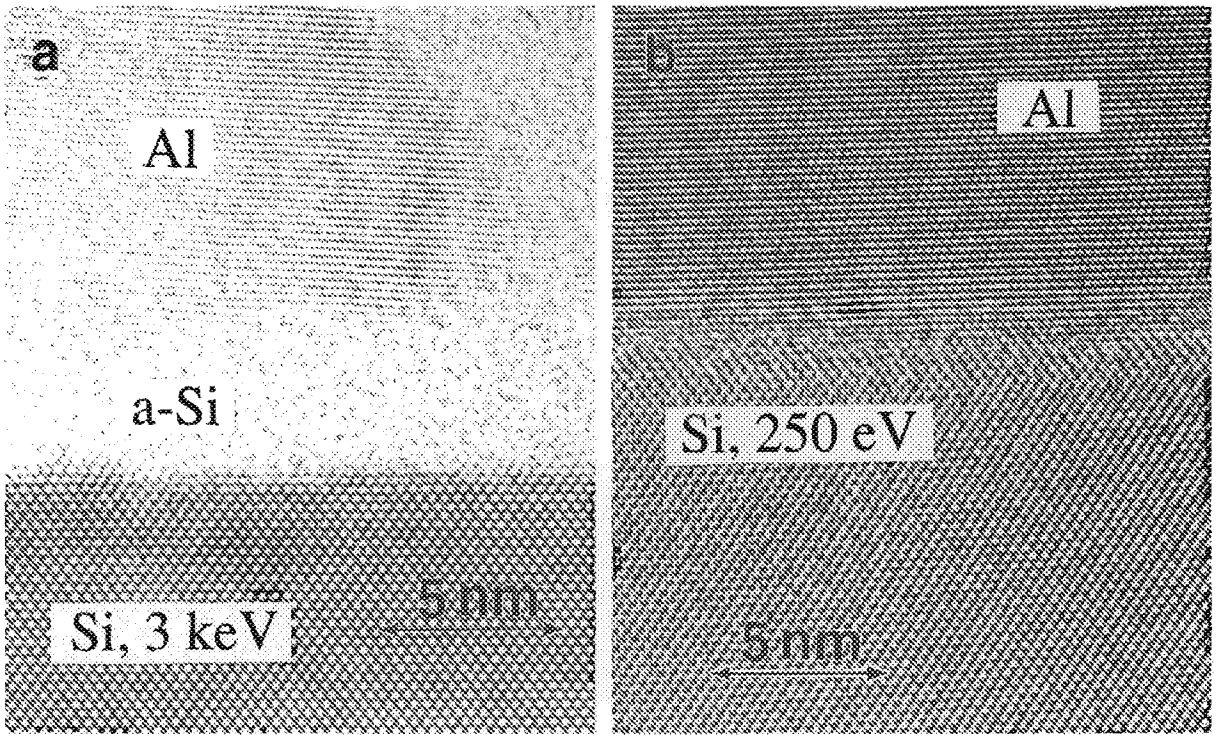

Fig. 7. Cross-sectional HREM images of silicon bombarded by Ar ion (a) at 3 keV, (b) at 250 eV covered by an Al protective layer in both cases.

However, this can hardly be justified since oxidation or any other source of contamination of the thinned TEM sample can contribute to the damage; e.g. an amorphous edge can typically be observed in images of cleaved specimens as well. Considering the above, we have decided to investigate the extent of the damage created by ion bombardment on covered samples preserving in this way the as-bombarded structure.

A new technique and arrangement (Barna et al., 1998) was applied for the quantitative determination of the amorphized thickness dependence on ion energy, as shown in Fig. 6. The basic idea is to cover, in situ, the bombarded surface with a protective layer and thus eliminate (as far as possible) oxidation and surface diffusion which occur during the sample "fabrication" for further study.

(100) faces of Si and GaAs single crystals were bombarded with Ar^+ ions at an angle of incidence $\gamma = 5°$ ($\Theta = 85°$ with respect to the surface normal). The ion energy was varied from 0.125 to 3 keV using the hot- and cold-cathode Teletwin guns. The fresh, ion bombarded surface was covered with an evaporated metal film of thickness in this way ≈ 30 nm (see Fig. 6(a)). Actually, metal deposition was started before the end of ion bombardment; to avoid the condition of "ion assisted deposition". The applied metal flux was at least two orders of magnitude higher than the ion flux (Hirvonen, 1995). The single-crystalline/amorphous/metal layer system was prepared as a cross section sample by our standard procedure (Barna, 1992). The main steps of the procedure are shown in Fig. 6(b) and (c). Al or Sn were used as protective metal layers. The temperature during the XTEM sample preparation did not exceed 170°C. Since neither metal-induced crystallisation of the amorphous Si film in the presence of the Al layer (Radnóczi et al., 1991), nor any change of the shape of the Sn crystal grains (218°C melting point) has been found (Barna et al., 1997), we believe that the sample temperature was sufficiently low during the ion milling. TEM sample preparation started with 10 keV Ar ions to remove most of the material and the ion energy was decreased to 3 keV before perforation of the samples. The cross-sectional TEM sample preparation was finished at the same energy that was used initially for the surface bombardment. The length of this bombardment was half an hour at least, thus the damage formed at higher energy was removed by the low energy Ar ions.

The amorphized layer thickness has been determined by HREM using either a Philips CM20 electron microscope with a normal twin objective lens or a JEOL 4000 EX. The [011] zone axis of the ion bombarded single crystals (GaAs, Si) was tilted parallel to the electron beam for the investigation. Measurement of the amorphised thickness was performed only when both the substrate and some metal grains could be resolved simultaneously.

Fig. 7 shows an Ar^+ implanted Si surface covered by an Al protective layer and prepared in cross-section. (The images were taken in a JEOL 4000 EX TEM.) In Fig. 7(a) the formation of a 4-nm thick amorphous silicon layer can be seen as a result of Ar^+ ion bombardment at 3 keV. The

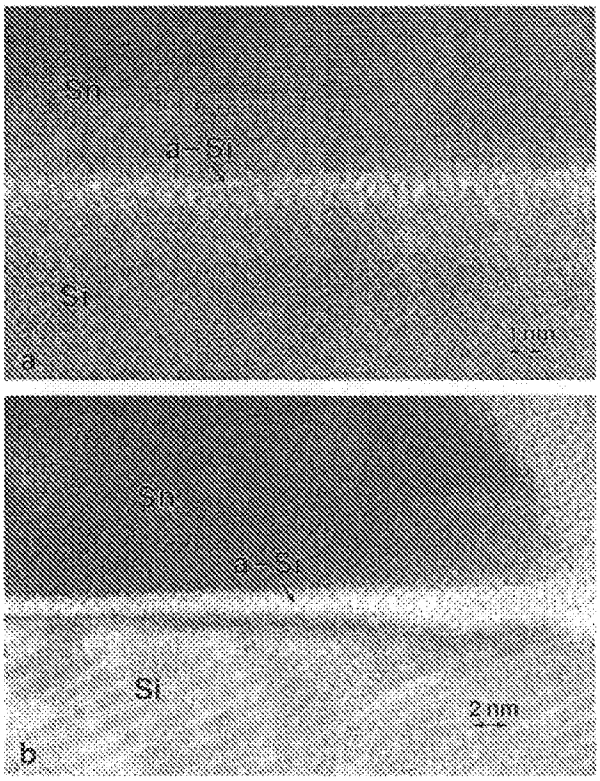

Fig. 8. Cross-sectional HREM images of silicon bombarded by Ar ions at 125 eV. The sample was covered by Sn. (a) beneath the Sn protective layer, (b) at the periphery of the Sn protective layer.

surface roughness of the bombarded silicon surface also evident (on the left side of the figure). The damaged layer thickness decreased when applying Ar^+ ions at 250 V as shown in Fig. 7(b). At certain parts of the sample the damage appears as a disturbed lattice (Fig. 7(b)) while at other regions a 1 nm thick amorphous layer was observed between the crystalline silicon and aluminium (Barna et al., 1998). The appearance of the damaged layer depends on the thickness of the part of the sample that is probed during the HREM study.

Fig. 8(a) shows a characteristic cross-sectional micrograph of the (001) Si surface after bombardment with 125 eV Ar^+ ions. The protective metal layer was Sn in this case. The amorphised thickness was approximately 2 monolayers (ML). These kind of experiments should be carried out with great care. When the protective layer is not continuous one cannot exclude an oxidation process during sample fabrication. Fig. 8(b) shows the aforementioned case; the substrate and the ion bombardment was same as before, but the Sn protective metal layer was not continuous (island structure). The thickness of the amorphous layer changed along the metal island; its thickness was more than twice as large at the perimeter, compared to under the Sn island (far from the middle of the island). This means that the Sn islands could not protect the silicon surface from further lateral oxidisation.

Fig. 9(a) shows an example of GaAs, bombarded at 1.6 keV with Ar ions. The amorphous layer thickness was about 2 nm. This is not too much for the usual HREM study,

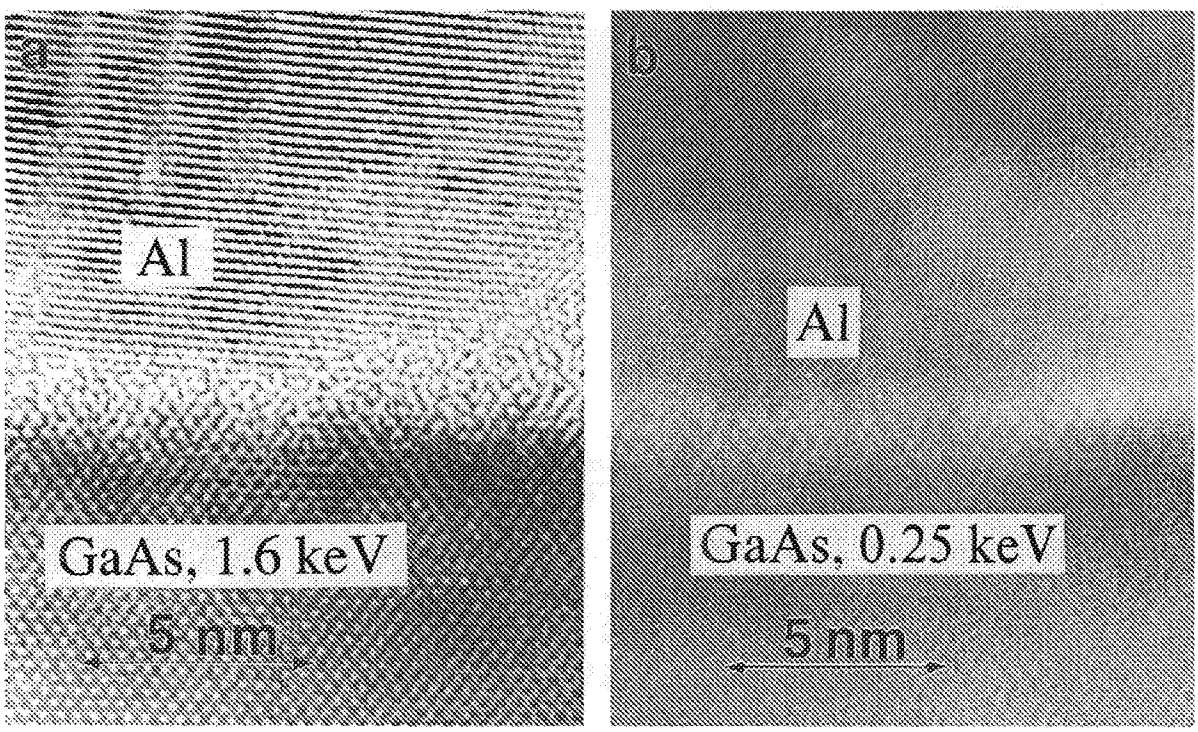

Fig. 9. Cross-sectional HREM images of GaAs bombarded by Ar ions (a) at 1.6 keV (the image was taken at 400 keV) and (b) at 250 eV (the image was taken at 200 keV).

but can be further decreased. For the case of Ar-ion bombardment at 250 eV (Fig. 9(b)) we could not detect any amorphous region between the GaAs crystalline surface and the Al protective layer (Barna et al., 1998). The fact that GaAs TEM samples can be prepared with a thinner damaged layer than silicon samples is due to the fact that GaAs is less sensitive to oxidisation.

Both the a-Si/Al and the a-Si/(001) Si interfaces show roughening of about 6 ML when bombarded with Ar^+ ions at 3 keV. Similar roughening of the interfaces was observed on GaAs, bombarded at lower (1.6 keV) ion energy (3–4 ML). The interface roughening between the substrate crystal and amorphised top layer was investigated in earlier XTEM measurements (Bulle-Lieuwma and Zalm, 1987; Yokota et al., 1990 etc.). However the free surface of the amorphized top layer was found to be atomically smooth. According to our measurements this might be the consequence of an oxidation process or viscous flow (Chason et al., 1994). In our experiments both phenomena are hindered. Roughening was not observed on GaAs and silicon surfaces (Barna et al., 1998) bombarded with Ar^+ ions at 250 eV (at $\Theta = 85°$); the decrease of surface roughness results in a clear HREM image with homogeneous contrast.

4. Conclusions

In this work we have shown that improved-quality HREM samples can be prepared by reduction of the ion energy to the range of 125–250 eV during the final stage of ion milling. This improvement is due to a reduction in the damaged-layer thickness and hindering of surface roughening. Samples sensitive to oxidisation cannot be prepared without an amorphous covering layer, which also avoids surface roughening and results in better images as well.

Contradictory ion beam damage results can be found in the literature, due to poorly defined experimental conditions (ion content, difference between the nominal and actual ion energy).

The dependence of ion beam damage on the angle of incidence should be investigated in the range of grazing angles.

Acknowledgements

Financial support of the OTKA Grant No. T025928 and T015880 as well as AKP No. 96/23 are acknowledged.

References

Barber, D.J., 1993. Radiation damage ion-milled specimens: characteristics, effects and methods of damage limitation. Ultramicroscopy 52, 101–125.

Barna, Á., Reisinger, G., Zsoldos, L., 1988. Ionenquelle für eine Einrichtung zur Ionenstrahl- bearbeitung, insbesondere zur Bearbeitung von Festörperproben. Eu. Patent N 141, 272.

Barna, Á., Barna, B.P., Zalar, A., 1990. Analysis of the development of large area surface topography during ion etching. Vacuum 40, 115–120.

Barna, Á., 1992. Topographic kinetics and practice of low angle ion beam thinning. Mater. Res. Soc. Symp. Proc. 254, 3–22.

Barna, Á., Menyhard, M., 1994. Auger depth profile analysis of deeply buried interfaces. Phys. Stat. Sol. (a) 154, 263.

Barna, Á., Szigethy, D., 1996. Patent No. PCT/HU96 /00054.

Barna, Á., Radnóczi, G., Pécz, B., 1997. Preparation techniques for transmission electron microscopy. In: Amelinckx, S. (Ed.), Handbook of Microscopy, 3. VCH Verlag, pp. 751–801.

Barna, Á., Pécz, B., Menyhárd, M., 1998. Amorphisation and surface morphology development at low energy ion milling. Ultramicroscopy 70, 161–171.

Benaissa, M., Humbert P., Ehret, G., Bensmina, F., 1994. Cleaved Si substrate wedges for thin film sandwich TEM observations. Proc. of ICEM-13, Paris, pp. 1029–1030.

Biersack, J.P., 1993. The effect of high charge states on the stopping and ranges of ions in solids. Nucl. Instr. Meth. B 80/81, 12–15.

Biersack, J.P., 1995. In: Pauleau, Y. (Ed.), The Physical Foundations of Ion Beam Interaction with Solids, NATO ASI Series, 290. Kluwer Academic, Dordrecht, pp. 39–65.

Brown, P.D., Humphreys, C.J., 1998. Electron microscopy, electrical activity, artefacts and the assessment of semiconductor epitaxial growth. Mater. Res. Symp. Proc. 523, 207–224.

Buckner, J.L., Vitkavage, D.J., Irene, E.A., 1988. Ellipsometric and Rutherford backscattering characterization of low-energy hydrogen-, helium-, and argon-bombarded silicon. J. Appl. Phys. 63, 5288–5294.

Buffat, P.A., Ganiere, J.D., Stadelmann, P., 1988. In: Cherns, D. (Ed.), Evaluation of Advanced Semiconductor Materials by Electron Microscopy, NATO ASI Series B, 203. Plenum Press, 319–334.

Bulle-Lieuwma, C.W.T., Zalm, P.C., 1987. Suppression of surface topography development in ion-milling of semiconductors. Surf. Interface Anal. 10, 210–215.

Carpenter, J.C.G, Jackman, J.A., McCaffrey, J.P., Alani, R., 1995. In situ hydride formation in zirconium and titanium during ion milling. J. Mic. Soc. America 1, 175–184.

Carter Jr., C.H., Davis, R.F., Nutt, S.R., 1986. Transmission electron microscopy of process-induced defects in β-SiC thin films. J. Mater. Res. 1, 811.

Chason, E., Mazer, T.M., Kellerman, B.K., McHroy, D.T., Howard, A.J., 1994. Roughening instability and evolution of the Ge(001) surface during ion sputtering. Phys. Rev. Lett. 72, 3040–3043.

Crocken, C.G., 1972. A glow discharge ion gun for etching. Vacuum 23, 11–13.

Hirvonen, J.K., 1995. In: Pauleau, Y. (Ed.), Ion Beam Assisted Thin Film Deposition, NATO ASI Series, 290. Kluwer Academic, Dordrecht, pp. 307–346.

Hu, Y.Z., Andrews, J.W., Li, M., Irene, E.A., 1991. In situ spectroscopic ellipsometric investigation of argon ion bombardment of single-crystal silicon and silicon dioxide films. Nucl. Instr. Meth. Phys. Res. B59/60, 76–79.

Hytch, M.J., Chevalier, J.P., 1994. The effect of amorphous surface layers on HREM images of crystalline material. Proc. of ICEM 13, Paris, 1994, pp. 367–368.

Ishiguro, T., Suzuki, T., Suzuki, N., Ozawa, M., 1987. Structure modification of surface layer induced by ion milling. J. Electron Microsc. 36, 163–167.

Ivey, D.G., Piercy, G.R., 1987. Radiation damage effects in GaAs transmission electron microscopy specimens prepared by ion milling. Thin Solid Films 149, 73–83.

Kawabe, M., Kanzaki, N., Masuda, K., Namba, S., 1978. Effect of ion etching on the properties of GaAs. Appl. Optics 17, 2556–2561.

Kestel, B., 1995. Specimen preparation: The Achilles heel of microscopy. In: Bailey, G.W., Ellisman, M.H., Hennigar, R.A., Zaluzec, J. (Eds.),

Proc. Microscopy and Microanalysis, Jones and Begel, New York, pp. 680–681.

Kido, Y., Nakano, H., 1990. Dose dependence of surface damage profiles for Ge(111) irradiated with 3 keV Ar^+. Surf. Sci. 239, 254–260.

Konomi, I., Kawano, A., Kido, Y., 1989. Damage profiling of Ar^+ irradiated Si(100) and GaAs(100) by medium energy ion scattering. Surf. Sci. 207, 427–440.

Malherbe, J.B., 1994. Sputtering of compound semiconductor surfaces. I. Ion-solid interaction and sputtering yields. Crit. Rev. Solid State Mater. Sci. 19, 55–127.

Malherbe, J.B., 1994. Sputtering of compound semiconductor surfaces. II. Compositional changes and radiation-induced topography and damage. Crit. Rev. Solid State Mater. Sci. 19, 129–195.

Markwitz, A., Klein, S., Michelmann, R.W., Baumannn, H., Krimmel, E.F., Bethge, K., 1996. Layer and interface analysis of ultra thin ion beam produced silicon nitride layers by NRA and TEM. Nucl. Instr. Meth. Phys. Res. B122, 284–288.

Menyhard, M., 1999. High-depth-resolution auger depth profiling atomic mixing. Micron 30, 255–265.

Pearton, S.J., Chakrabarti, U.K., Perley, A.P., Jones, K.S., 1990. Ion milling damage in InP and GaAs. J. Appl. Phys. 68, 2760–2768.

Radnóczi, G., Robertsson, A., Hentzell, H.T.G., Gong, S.M., Hasan, M.A., 1991. Al induced crystallization of a-Si. J. Appl. Phys. 69, 6394.

Schuhrke, T., Mändl, M., Zweck, J., Hoffman, H., 1992. Investigation of surface amorphization of silicon wafers during ion milling. Ultramicroscopy 41, 429–433.

Walker, J.F., Broom, R.F., 1997. Surface damage of semiconductor TEM samples prepared by focused ion beams. Inst. Phys. Conf Ser. 157, 473–478.

Yokota, Z., Hashimoto, H., Song, M., Awai, M., 1990. Surface topography of ion-etched Si wafers studied by electron microscopy. Jap. J. Appl. Phys. 29, 739–743.

Zalm, P.C., Vrizema, C.J., 1992. On some factors limiting depth resolution during SIMS profiling. Nucl. Inst. Meth. Phy. Res. B67, 495.